JACS
JOURNAL OF THE AMERICAN CHEMICAL SOCIETY
pubs.acs.org/JACS
Article

Photostimulated Spiropyran for Instantaneous Visualization of Thermal Field Distribution and Flow Pattern

Yahui Chen, Yefei Liu, Sheng Lu, Shuang Ye, Hao Gu, Jian Qiang, Yourong Li,* and Xiaoqiang Chen*

Cite This: https://dx.doi.org/10.1021/jacs.0c09460 Read Online

ACCESS | Metrics & More | Article Recommendations | Supporting Information

ABSTRACT: The study of thermocapillary convection has attracted the attention of researchers due to the importance in both fundamental and industrial aspects. To trace the state of flows in real time during thermocapillary convection, the development of imaging methods and tools is essential. Here we use a benzothiazole unit-bearing spiropyran (**BS1-SP**) as a photostimulated indicator to visualize the details of instantaneous temperature distribution and flow pattern on the surface of volatile solvent simultaneously with a high spatial and temporal resolution during convection. This work provides insights into dynamic self-organization and thermo-hydrodynamics taking place in evaporating systems, and a useful tool to study these behaviors.

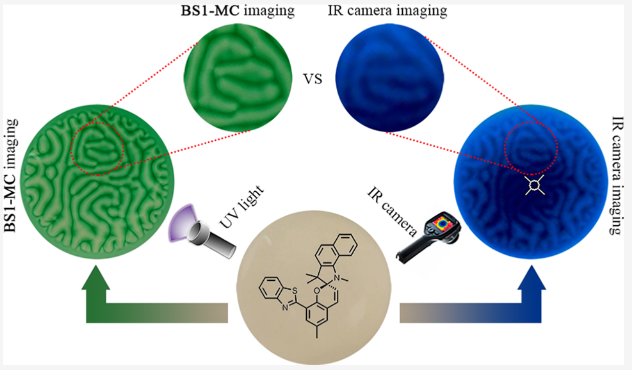

INTRODUCTION

The thermocapillary convection is commonly involved in various industrial processes such as crystal growth,[1,2] droplet evaporation,[3,4] and microfluidics.[5] The understanding of the dynamic behaviors of flows during thermocapillary convection becomes very important in both fundamental and industrial aspects. Especially, the dynamic behaviors of flows driven by a horizontal temperature gradient in fluid layers with a free upper surface have attracted the attention of the researchers for many years.[6] Many experiments have been designed and carried out in liquid pools with various geometries to investigate the relationships between the dynamic behaviors of flows and environmental parameters.[7−11] Over the course of these experiments, some measurement methods and tools are developed to obtain information on the state of flows. For instance, infrared cameras, thermo-chromic liquid crystals, and phosphorescence-based visualization techniques are common optical tools used for two-dimensional temperature measurement;[12] the conjunction technology of particle image velocimetry and polystyrene fluorescent particles are employed to trace the patterns of the thermocapillary flows.[13] However, until now, it has been rather challenging to observe the details of instantaneous temperature distribution and flow patterns simultaneously with a high spatial and temporal resolution during thermocapillary convection.

Spiropyran derivates are a class of molecules that can transit between a parent ring-closed isomer of spiropyran (SP) and a ring-open isomer of merocyanine (MC) upon external stimuli such as temperature, UV/vis light, acidity, environmental polarity, and mechanical stress.[14] The two isomers show vast differences in physicochemical properties including molecular polarity and conformation, and optical properties.[15−17] Because of the reversible isomerization and unique properties of the isomers, spiropyran has been widely utilized as a molecular switch in the construction of dynamic materials in a various range of applications.[18−20] In the study described below, we found that the UV-irritated isomerization of a spiropyran derivate (**BS1-SP**) generated colored self-organization aggregates, precisely located at the cold regions on the surface of volatile solvents. On the basis of the discovery, we developed a method to realize the instantaneous visualization of thermal field distribution and thermocapillary flows during the evaporation of solvents and explored the application of **BS1-SP** in imaging the fluid thermodynamics.

RESULTS AND DISCUSSION

Two spiropyrans **BS1-SP** and **BS2-SP** (Figure 1A) were initially prepared using the routes depicted in Scheme S1 of the Supporting Information. The structures of these substances were assigned by using NMR spectroscopy and high-resolution mass spectrometry (Figures S10−S30). The conversions of **BS1-SP** to **BS1-MC** promoted by irradiation with UV-light are shown in Figure 1B. We observed that UV light irradiation of **BS1-SP** in dichloromethane (DCM) promotes the formation of green color in association with the growth of a visible absorption

Received: September 2, 2020

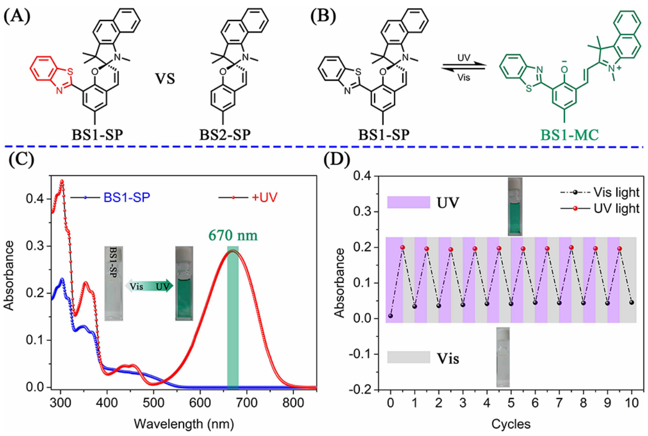

Figure 1. Isomerization and optical properties of the **BS1** system. (A) Molecular structures of **BS1-SP** and **BS2-SP**. (B) Interconversion between **BS1-SP** and **BS1-MC**. (C) Blue line: absorption spectrum of **BS1-SP** in DCM. Red line: absorption spectrum of UV-irradiated solution of **BS1-MC**. (D) Repeated interconversion between the two isomers of **BS1** molecules (absorption at 670 nm) in DCM solution under UV light irradiation and Vis light condition, showing the good fatigue resistance. Concentration: 20 μM.

band at 670 nm, indicating the formation of the zwitterionic **BS1-MC** (Figure 1C). The emergence and disappearance of green color can be reversibly controlled by exposure to UV light or daylight (Figure 1D). In contrast, UV-light irradiation does not promote observable isomerization of the ring-closed form of the nonbenzothiazole containing spiropyran **BS2-SP** to the ring-opened form **BS2-MC** (Figure S1). Thus, the presence of the benzothiazole moiety increases the stability of merocyanine zwitterion.

The photostimulated color transition of **BS1-SP** in DCM was then investigated in detail. When DCM solution containing **BS1-SP** in a disk was subjected to UV irradiation (365 nm), a green worm-like pattern associated with **BS1-MC** generated on the surface of the solvent (Figure 2A and Video S1). Surprisingly, we found that the worm-like markings are identical to the distribution of the thermal field on the surface of DCM observed with an infrared camera (Figure 2A). Obviously, the green **BS1-MC** aggregates are located in the cold area of volatile DCM. Moreover, in contrast to the infrared image, the **BS1**-based system visualizes the thermal field with a much higher resolution. The similar phenomenon was also found on the surface of volatile chloroform ($CHCl_3$), 1-bromopropane (1-BP), and 1,2-dichloroethane (DCE), respectively (Figure S2). We further speculated the mechanism of **BS1-SP** imaging the cold area of volatile DCM. In an open solvent system with a free upper surface, the evaporation of DCM leads to the uneven temperature distribution on the surface of the solvent. Because of the higher surface tension on the low temperature area, **BS1-SP** molecules on the surface of the solvent are prone to aggregate spontaneously at the low-temperature area for keeping the balance between the surface tension at the high and low-temperature areas. Upon the irradiation of UV light, the concentrated **BS1-SP** turns to green **BS1-MC** on the cold regions of the solvent surface (Figure 2B).

The patterns observed for **BS1-SP** aggregates are identical to the distribution of a thermal field, which is also related to the convection inside a liquid. Thus, we anticipated that the shape of the container might also impact the thermal field distribution on the surface of an evaporating solvent. To assess this possibility,

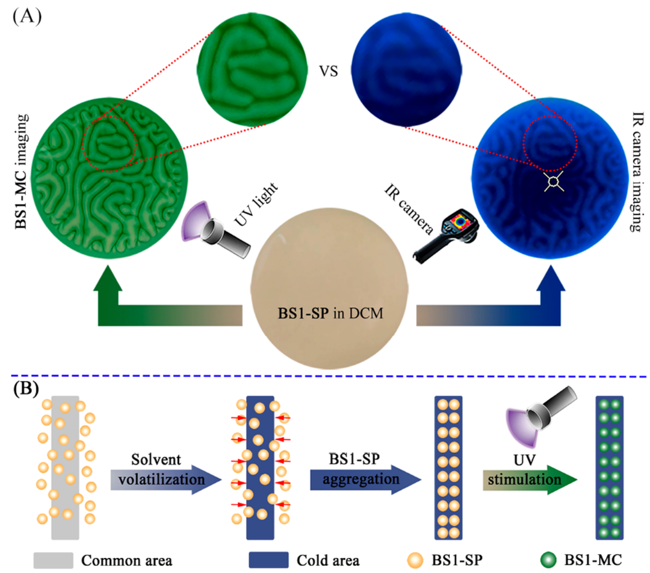

Figure 2. (A) Worm-like pattern of **BS1-MC** formed on the surface of volatile DCM after irradiation using UV light (left, green pattern); the worm-like temperature distribution on the surface of volatile DCM captured by an infrared camera (right, blue pattern). (B) Proposed mechanism for thermal field distribution imaging by **BS1-MC**. Initially, the **BS1-SP** molecules distribute randomly on the surface of solvent; the volatilization of DCM leads to the uneven temperature field; the **BS1-SP** molecules move to cold area due to the surface tension; upon the irradiation of UV light, the generated green **BS1-MC** visualizes the cold area.

an agate mortar was used as the container for pattern formation in DCM. Different from the pattern formed in disk, upon UV irradiation, a flower-like green pattern was generated on the surface of DCM (Figure 3A). After the UV light was removed,

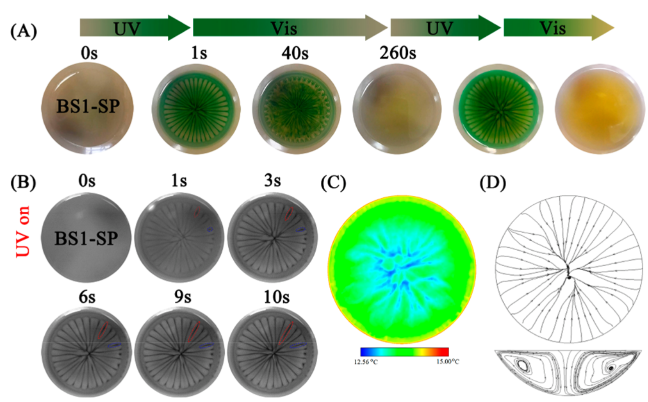

Figure 3. Flower-like pattern formation of **BS1-MC** driven by convection. (A) In a mortar, **BS1-SP** (2 mM) in DCM is irradiated using UV light for 1 s to form the green flower-like pattern associated with **BS1-MC** on the surface of DCM. The pattern and color fade when the solution is exposed to visible light. And the flower-like pattern formed by UV light irradiation of **BS1-SP** in DCM and its disappearance under visible light with a repeatable mode. (B) Two streams (red and blue dashed cycles) that reveal the formation of **BS1-SP** aggregates at the edge of the solvent, followed by translocation of the aggregates to the center area driven by the convective flows. (C) Temperature distribution on the free DCM surface determined by the numerical simulation. (D) Streamlines on the free surface (top) and a meridian plane (bottom) for DCM liquid determined by the numerical simulation.

https://dx.doi.org/10.1021/jacs.0c09460
J. Am. Chem. Soc. XXXX, XXX, XXX−XXX

the green color and flower-like pattern faded with time, in conjunction with the conversion of **BS1-MC** to colorless **BS1-SP** (Figure 3A and Video S2). The formation and disappearance of the green flower-like pattern can be reversibly controlled with UV light "ON" and "OFF" (Figure 3A). By using the high-speed camera, we observed that the green color associated with **BS1-MC** formed at the wall of the mortar, and then streamed toward the center of the solution, eventually forming the flower-like pattern on the surface of the solution (Figure 3B, Video S3). The results suggest that the green flower-like pattern formed by UV irradiation of **BS1-SP** is a consequence of the patterned distribution of self-aggregates of **BS1** molecules on the surface of DCM driven by the surface tension and convections. Additionally, we also observed the formation of a flower-like pattern of **BS1-SP** solids at the bottom of the mortar after evaporation of DCM without UV irradiation, indicating the patterned aggregation of **BS1** molecules on the surface of DCM is irrelevant to UV irradiation (Figure S3).

We speculated that the thermal fields at the evaporating DCM surface induce convective flows via the Marangoni effect, which serves as the driving force for pattern formation. To support this proposal and gain insights into the mechanism of pattern formation, dynamics simulations were carried out by using the finite volume method. The simulation results demonstrate that the calculated temperature distribution on the surface of DCM is similar to that observed experimentally by using an infrared camera (Figure 3C and Figure S4). The nonuniform temperature distribution is a result of evaporative cooling, where heat loss caused by evaporation of DCM is supplemented rapidly from solvent at the periphery of the container, leading to a higher temperature than that of the central region. Because a lower temperature of the solvent is associated with a higher surface tension, a surface tension gradient is generated that drives liquid flow from the periphery to the central region (Figure 3D, top). This is consistent with the observed direction that the **BS1-MC** stream follows during the process of pattern formation (Figure 3B and Video S3). The simulated streamlines on a meridian plane suggest that the cooler solvent in the central region descends to the mortar bottom and circle back to the liquid periphery, creating a loop of convective flow (Figure 3D, bottom). It is important to point out that surface evaporation causes the formation of a large negative vertical temperature gradient, resulting in instability of the flows near the periphery of the free surface of the liquid. This phenomenon induces the formation of a group of convective cells with an opposite rotational direction near the periphery (Figure 3 D, bottom), which spread toward the central region by the thermocapillary flow on the free surface. As expected, when the agate mortar was covered by a transparent glass to suppress the evaporation, the UV irradiation of **BS1-SP** DCM solution led to the formation of a uniformly distributed green color at the surface of the solution instead of generating a flower-like pattern (Figure S5). Therefore, it appears that the flower-like pattern is a consequence of Rayleigh-Benard-Marangoni instability. This is the reason why the green **BS1-MC** self-organization region overlaps with the area of low temperature, resulting in the formation of the "flower petals" profile.

Given that the formation of patterned self-aggregates of **BS1-MC** on the surface of DCM is closely related to the convection status of the solvent in the mortar, when the temperature is <0 °C, the surface of DCM exhibits an evenly distributed thermal field (Figure S6). Convection does not take place at this temperature because the driving force arising from buoyancy is too weak to overcome the viscous resistance of DCM. As a consequence, no flower-like pattern formed at this temperature. When the temperature rises to 4 °C, convection becomes strong enough to support the formation of a flower-like patterned thermal field (Figure S6 and Video S4). However, a further increase in the temperature leads to a disordered **BS1-MC** pattern because the intense convection leads to the disruption of the ordered thermal field on the surface of DCM (Figure S7 and Video S5). These findings suggest that a moderate surface evaporation rate is needed to create a stable pattern of **BS1-MC** self-aggregates. Meanwhile, we found that the concentration of **BS1-SP** from (0.1 mM to 10 mM) barely affected the thermal distribution at the surface of DCM (Figure S8), demonstrating that the visualization of convective flows using **BS1** method reflects the intrinsic property of the solvent.

We further considered whether the patterned **BS1-MC** self-aggregates can be tuned by changing the environmental parameters and the solvent properties. When placing the cold source on one side of the mortar, the patterned **BS1-MC** self-aggregates showed an off-centered convergence point, which was closer to the location of the cold source. The pattern was restored to the symmetric shape after the removal of the cold source (Figure 4A and Video S6). Besides, we investigated the formation of flower-like patterns by **BS1-MC** in different haloalkane solvents including 1-BP, $CHCl_3$, and DCE. We observed that the flower-like patterns generated in these solvents contain different numbers of petals (Figure 4B). Fewer petals were found to associate with the solvent with a higher viscosity. Since the temperature and the viscosity of the solvent are two key parameters that govern the driving force and resistance to the formation of the self-assembled patterns, we tried to describe the relationship between the number of petals and the two parameters of the above halogenated alkanes by establishing an equation below,

$$N = \mathrm{A}[-(\delta\gamma/\delta T)\times \Delta T/\mu]^{\mathrm{m}}$$

where N is the number of petals, which is dimensionless; $\partial\gamma/\partial T$ is the change rate of surface tension coefficient with temperature; ΔT denotes the temperature difference between the periphery and the center; and μ is the dynamic viscosity of the solvent. The values of $\partial\gamma/\partial T$ and μ for each solvent were obtained from the Lange's Handbook of Chemistry[21] (Figure 4C). The plot of ln N versus ln $(-(\partial\gamma/\partial T) \times \Delta T/\mu)$ (Figure 4D) shows a linear relationship between ln N and ln $(-(\partial\gamma/\partial T) \times \Delta T/\mu)$. These results also demonstrated that the distribution of benzothiazole-bearing spiropyran molecules and flow patterns on the solvent surface can be tuned by changing the local temperature and solvent properties.

■ CONCLUSION

In summary, we developed a benzothiazole-bearing spiropyran derivate **BS1-SP** that served as an excellent photoactivated probe for visual observation of temperature distribution occurring on the surfaces of evaporating organic solvents. Furthermore, Rayleigh-Benard-Marangoni convective flows on the surface of evaporating DCM can be visualized by the self-aggregation of **BS1-MC**, which is produced by UV-irradiation induced ring-opening of **BS1-SP**. Also, we tried to manipulate the patterned **BS1-MC** self-aggregates on the surface of solvents by changing the local temperature and the properties of the solvents. The observations made in this effort give new insights into the dynamic self-organization and hydrodynamics taking place in evaporating systems. This work also provides a useful

https://dx.doi.org/10.1021/jacs.0c09460
J. Am. Chem. Soc. XXXX, XXX, XXX−XXX

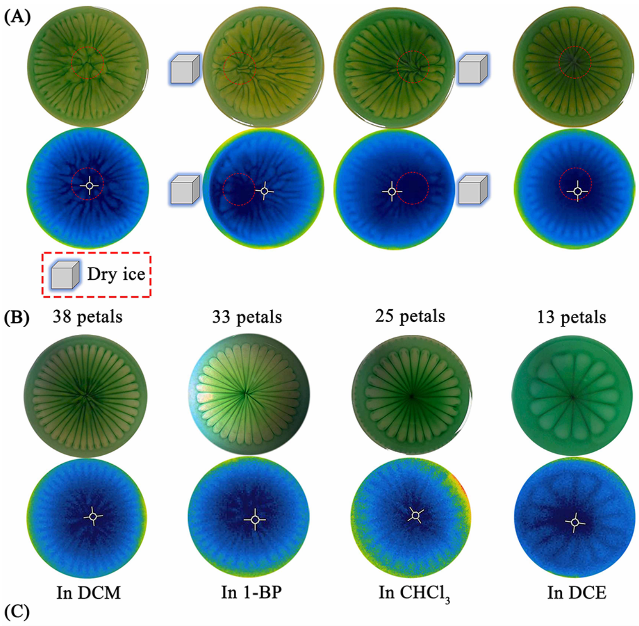

(C)

Solvents	$-(\partial\gamma/\partial T)$	ΔT (°C)	μ (mN·s·m^{-2})	$-(\partial\gamma/\partial T)\times\Delta T/\mu$	N	$\ln(-(\partial\gamma/\partial T)\times\Delta T/\mu)$	$\ln N$
DCM	0.1284	2.00	0.449	0.57	38	-0.56	3.64
1-BP	0.1218	1.80	0.539	0.41	33	-0.89	3.50
$CHCl_3$	0.1295	1.70	0.596	0.37	25	-0.99	3.22
DCE	0.1428	1.50	0.917	0.23	13	-1.47	2.56

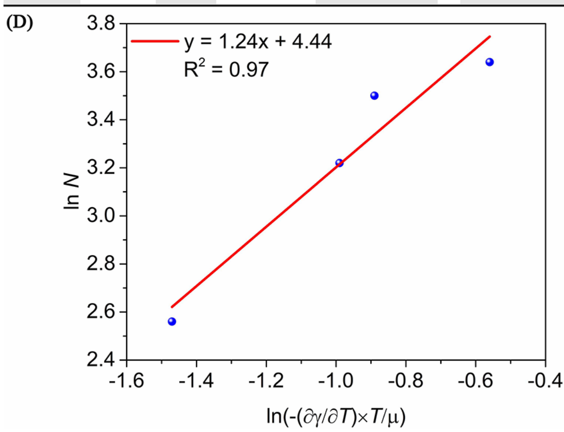

Figure 4. Effects of local cooling and solvent properties on flower-like pattern formation. (A) Patterns imaged by **BS1-SP** (upper row) and infrared camera images (lower row) of the surface of evaporating DCM. From left to right: no dry ice around the mortar; dry ice on the left side of mortar; dry ice on the right side of the mortar; dry ice removed. (B) Flower-like patterns in different solvents were imaged by the **BS1-SP** system (upper row) and their infrared images (lower row). From left to right: DCM; 1-BP; $CHCl_3$; DCE. (C) Physical parameters of solvents and the corresponding numbers of petals. (D) Linear relationship between ln N and $\ln(-(\partial\gamma/\partial T) \times \Delta T/\mu)$.

tool for real-time imaging of temperature distribution and flow patterns on the surfaces of evaporating solvents.

■ ASSOCIATED CONTENT

Supporting Information

The Supporting Information is available free of charge at https://pubs.acs.org/doi/10.1021/jacs.0c09460.

Chemicals and apparatus; synthesis routes of compounds **BS1-SP** and **BS2-SP**; preparation of samples; absorption spectrum of **BS2-SP** in DCM solution; formation of "worm-like pattern" in $CHCl_3$, 1-BP, and DCE; formation of flower-like pattern after DCM evaporation completed; flower-like temperature field distribution of DCM collected by FILR infrared camera; flower-like pattern destroyed by preventing convection; flower-like pattern formed with increasing temperature; flower-like pattern w destroyed by increasing temperature; influence of **BS1-SP** concentration on formation of flow pattern; model formulation and numerical method; characterization of compounds (PDF)

Video of DCM solution containing **BS1-SP** in disk subjected to UV irradiation (MP4)

Video of conversion of **BS1-MC** to colorless **BS1-SP** (MP4)

Video of green color associated with **BS1-MC** formed at wall of mortar, then streamed toward center of solution, eventually forming flower-like pattern on surface of solution (MP4)

Video of convection strong enough to support formation of flower-like patterned thermal field (MP4)

Video of further increase in temperature leading to disordered **BS1-MC** pattern because intense convection leads to disruption of ordered thermal field on surface of DCM (MP4)

Video of pattern restored to symmetric shape after removal of cold source (MP4)

■ AUTHOR INFORMATION

Corresponding Authors

Xiaoqiang Chen − *State Key Laboratory of Materials-Oriented Chemical Engineering, College of Chemical Engineering, Jiangsu National Synergetic Innovation Center for Advanced Materials (SICAM), Nanjing Tech University, Nanjing 211816, China;* orcid.org/0000-0003-2493-2067; Email: chenxq@njtech.edu.cn

Yourong Li − *Key Laboratory of Low-grad Energy Utilization Technologies and Systems of Ministry of Education, School of Energy and Power Engineering, Chongqing University, Chongqing 400044, China;* Email: liyourong@cqu.edu.cn

Authors

Yahui Chen − *State Key Laboratory of Materials-Oriented Chemical Engineering, College of Chemical Engineering, Jiangsu National Synergetic Innovation Center for Advanced Materials (SICAM), Nanjing Tech University, Nanjing 211816, China*

Yefei Liu − *State Key Laboratory of Materials-Oriented Chemical Engineering, College of Chemical Engineering, Jiangsu National Synergetic Innovation Center for Advanced Materials (SICAM), Nanjing Tech University, Nanjing 211816, China*

Sheng Lu − *State Key Laboratory of Materials-Oriented Chemical Engineering, College of Chemical Engineering, Jiangsu National Synergetic Innovation Center for Advanced Materials (SICAM), Nanjing Tech University, Nanjing 211816, China;* orcid.org/0000-0003-0481-8531

Shuang Ye − *Key Laboratory of Low-grad Energy Utilization Technologies and Systems of Ministry of Education, School of Energy and Power Engineering, Chongqing University, Chongqing 400044, China*

Hao Gu − *State Key Laboratory of Materials-Oriented Chemical Engineering, College of Chemical Engineering, Jiangsu National Synergetic Innovation Center for Advanced Materials (SICAM), Nanjing Tech University, Nanjing 211816, China*

https://dx.doi.org/10.1021/jacs.0c09460
J. Am. Chem. Soc. XXXX, XXX, XXX−XXX

Jian Qiang − *State Key Laboratory of Materials-Oriented Chemical Engineering, College of Chemical Engineering, Jiangsu National Synergetic Innovation Center for Advanced Materials (SICAM), Nanjing Tech University, Nanjing 211816, China*

Complete contact information is available at:
https://pubs.acs.org/10.1021/jacs.0c09460

Notes

The authors declare no competing financial interest.

■ ACKNOWLEDGMENTS

This investigation was supported financially by the National Natural Science Foundation of China (21722605, 21978131, 51776022, 11532015), the National Key R&D Program of China (2018YFA0902200), the Natural Science Foundation of Jiangsu Province (SBK2020043221), the Six Talent Peaks Project in Jiangsu Province (XCL-034) and the Project of Priority Academic Program Development of Jiangsu Higher Education Institutions (PAPD).

■ REFERENCES

(1) Fang, H.; Tian, J.; Zhang, Q.; Pan, Y.; Wang, S. Study of melt convection and interface shape during sapphire crystal growth by Czochralski method. *Int. J. Heat Mass Transfer* **2012**, *55*, 8003−8009.

(2) Minakuchi, H.; Takagi, Y.; Okano, Y.; Gima, S.; Dost, S. The relative contributions of thermo-solutal Marangoni convections on flow patterns in a liquid bridge. *J. Cryst. Growth* **2014**, *385*, 61−65.

(3) MacDonald, B. D.; Ward, C. A. Onset of Marangoni convection for evaporating sessile droplets. *J. Colloid Interface Sci.* **2012**, *383*, 198−207.

(4) He, B.; Duan, F. Evaporation and convective flow pattern of a heated pendant silicone oil droplet. *Int. J. Heat Mass Transfer* **2015**, *85*, 910−915.

(5) Pan, Z.; Wang, F.; Wang, H. Instability of Marangoni toroidal convection in a microchannel and its relevance with the flowing direction. *Microfluid. Nanofluid.* **2011**, *11*, 327−338.

(6) Peng, L.; Li, Y. R.; Shi, W. Y.; Imaishi, N. Three-dimensional thermocapillary-buoyancy flow of silicone oil in a differentially heated annular pool. *Int. J. Heat Mass Transfer* **2007**, *50*, 872−880.

(7) Zhang, Q.-Z.; Peng, L.; Wang, F.; Liu, J. Thermocapillary convection with bidirectional temperature gradients in a shallow annular pool of silicon melt: Effects of ambient temperature and pool rotation. *Int. J. Heat Mass Transfer* **2016**, *101*, 354−364.

(8) Zhang, L.; Li, Y.-R.; Wu, C.-M.; Liu, Q.-S. Flow pattern transition and destabilization mechanism of thermocapillary convection for low Prandtl number fluid in a deep annular pool with surface heat dissipation. *Int. J. Heat Mass Transfer* **2018**, *126*, 118−127.

(9) Karapetsas, G.; Matar, O. K.; Valluri, P.; Sefiane, K. Convective Rolls and Hydrothermal Waves in Evaporating Sessile Drops. *Langmuir* **2012**, *28*, 11433−11439.

(10) Zhu, J.-L.; Shi, W.-Y.; Feng, L. Benard-Marangoni instability in sessile droplet evaporating at constant contact angle mode on heated substrate. *Int. J. Heat Mass Transfer* **2019**, *134*, 784−795.

(11) Sefiane, K.; Moffat, J. R.; Matar, O. K.; Craster, R. V. Self-excited hydrothermal waves in evaporating sessile drops. *Appl. Phys. Lett.* **2008**, *93*, 074103−074105.

(12) Yi, S. J.; Kim, M.; Kim, D.; Kim, H. D.; Kim, K. C. Transient temperature field and heat transfer measurement of oblique jet impingement by thermographic phosphor. *Int. J. Heat Mass Transfer* **2016**, *102*, 691−702.

(13) Chamarthy, P.; Dhavaleswarapu, H. K.; Garimella, S. V.; Murthy, J. Y.; Wereley, S. T. Visualization of convection patterns near an evaporating meniscus using mu PIV. *Exp. Fluids* **2008**, *44*, 431−438.

(14) Klajn, R. Spiropyran-based dynamic materials. *Chem. Soc. Rev.* **2014**, *43*, 148−184.

(15) Remon, P.; Li, S. M.; Grotli, M.; Pischel, U.; Andreasson, J. An acido- and photochromic molecular device that mimics triode action. *Chem. Commun.* **2016**, *52*, 4659−4662.

(16) Xie, X.; Mistlberger, G.; Bakker, E. Reversible Photodynamic Chloride-Selective Sensor Based on Photochromic Spiropyran. *J. Am. Chem. Soc.* **2012**, *134*, 16929−16932.

(17) Zhang, J.; Zou, Q.; Tian, H. Photochromic Materials: More Than Meets The Eye. *Adv. Mater.* **2013**, *25*, 378−399.

(18) Khazi, M. I.; Jeong, W.; Kim, J.-M. Functional Materials and Systems for Rewritable Paper. *Adv. Mater.* **2018**, *30*, 1705310−1705331.

(19) Samanta, D.; Galaktionova, D.; Gemen, J.; Shimon, L. J. W.; Diskin-Posner, Y.; Avram, L.; Kral, P.; Klajn, R. Reversible chromism of spiropyran in the cavity of a flexible coordination cage. *Nat. Commun.* **2018**, *9*, 641−649.

(20) Qi, Q.; Li, C.; Liu, X.; Jiang, S.; Xu, Z.; Lee, R.; Zhu, M.; Xu, B.; Tian, W. Solid-State Photoinduced Luminescence Switch for Advanced Anticounterfeiting and Super-Resolution Imaging Applications. *J. Am. Chem. Soc.* **2017**, *139*, 16036−16039.

(21) Dean, J. A. *Lange's Handbook of Chemistry*, 15th ed.; McGraw-Hill: New York, 1999.